Magnetic Characterization of Solvent Resistance in Vanadium Tetracyanoethylene V[TCNE]$_{x\sim2}$

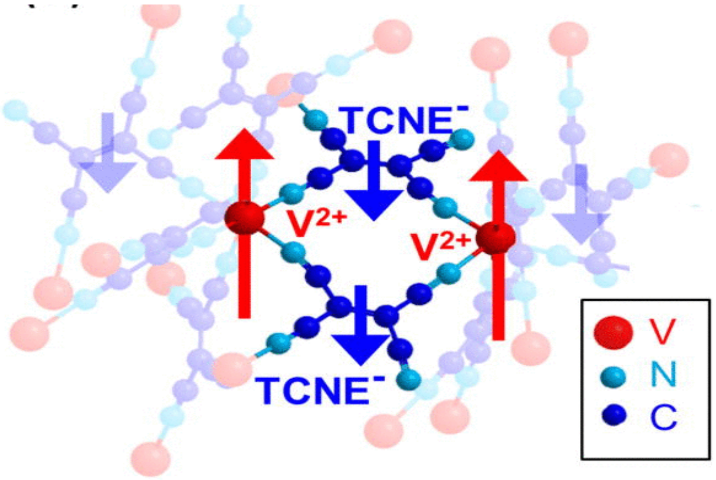

Sindy D, Lauricella[1]. Stephanie Lake.[2] Andrew Franson[2]. Michael Chilcote.[2] Yulia Getmanenko.[1] Ezekiel Johnston-Halperin.[2]

[1]New Mexico Highlands University

[2]Department of Physics. The Ohio State University

Abstract

Organic-based magnetic materials have beneficial applications such as electronic materials, room temperature magnetic ordering, and mechanical flexibility. The organic-based magnet we will be focusing on throughout this research is Vanadium tetracyanoethylene V[TCNE]$_{x\sim2}$, a semiconducting ferrimagnet that displays room temperature magnetic ordering. It is considered a metal organic hybrid system because it's combining an organic ligand with a metal atom. There are few projects that focus on different ways to analyze the limits of manipulating V[TCNE] one is replacing TCNE ligand with new ligands that are designed then adding dichloromethane to test weather the new ligands can make air-stable ferrimagnets. Another approach is adding solvents to metals and identify if there are any magnetic changes in the structure of V[TCNE]. This research will consist of synthesizing thin films of V[TCNE] with V(CO)6 and TCNE via Chemical Vapor Deposition (CVD) in a glass furnace. The grown CVD films decompose in air that result in loss of magnetic properties, which is why the process is done in an argon glove box. Once completed our V[TCNE] we will use the Superconducting Quantum Interference Device (SQUID) that helps identify the global magnetic ordering of the sample by measuring magnetization. SQUID will be used before adding a dichloromethane solvent to record the control measure of V[TCNE] and after the solvent is added. We are adding dichloromethane solvent to determine weather or not our V[TCNE] films are resistant to the solvent and see if there are changes in the magnetic field and in the microscopic scale. Electronic paramagnetic Resonance (EPR) will be used to identify what's inside the material and see how much change has occurred in the signatures. Signatures are peaks shown in the data that we will later review to identify if the material continues to have V[TCNE] after adding the dichloromethane solvent.

Background

Materials in magnetic ordering arise from changes between unpaired electrons. V[TCNE] has room temperature magnetic ordering and is a good asset in organic materials for magnetoelectronic applications including low cost manufacture. Some magnetic behaviors have no collective magnetic interactions and have no magnetic order such as diamagnetism and paramagnetism. Others have a long range of magnetic order and can be critical under certain temperatures; these types of behaviors are ferromagnetism and ferrimagnetism. As described before, V[TCNE] is a semiconducting ferrimagnet that has strong exchange interactions of oxygen ions that have antiparallel spins. This phase depends on the Curie temperature (Tc), which determines the temperature that a material loses magnetic ordering.

An antiferromagnetic material has no net magnetization and form opposite aligned spins that cancel each other out. A ferrimagnetic is similar to an antiferromegnet except the antiparallel spins on sublattices will not cancel out. This is calculated as $\mathbf{M} = \chi\mathbf{H}$ where χ = magnetic susceptibility. Ferromagnet and ferrimagnet systems that are above the Curie temperature perform as a paramagnet where χ is positive. When they experience a strong magnetic field all domains will align (Harberts, Megan). Below the Tc, ferromagnetic material spins are aligned and shows an overall net magnetization.

First step is making thin films of $V[TCNE]_{x\sim2}$ that are synthesized using Chemical Vapor Deposition. CVD is applied to prepare thin films from organic materials using a conventional hot-wall. In a glass tube we apply two vapor phase precursors that are used to create thin films of V[TCNE] which are vanadium hexacarbonyl ($V(CO)_6$) and tetracyanoethylene TCNE. ($V(CO)_6$) is used because it has less temperature dependent magnetization making CO being easily removed from vanadium (F. Author & S. Author). ($V(Co)_6$) reacts together to connect to one of the nitrogen ions of TCNE in the siano group. This means that vanadium connects to one nitrogen making that electron like the vanadium nitrogen more than the vanadium oxygen so then leaved the carbon to deposit itself as carbon dioxide.

We will first place our substrates towards the middle of the glass tube so argon can vent above them in order for the TCNE and (V(CO)6) to deposit into the substrates. Then we will add 1.0 g of TCNE in a small glass boat and place it on the left end of the glass and 4.5 mg of (V(CO)**6**) on the right side in a T-boat. Next, we place TCNE to the hottest part in the reactor that is roughly 65°C, then we raise an oil bath to the T-boat of $(V(CO)_6)$ that is 10°C and open a vacuum line connected beneath the pressure gauge to 30-60 mmHg. Once we set a flow rate of 65 sccm for (V(CO)**6**) and 95 sccm of TCNE the reaction should occur within an hour after the time of deposition, allowing both to interact with each other and creating successful film growths of V[TCNE] (Harberts et al. (2015). Figure 1 shows the final result of V[TCNE] film growths.

Figure 1. Six V[TCNE] film growths.

Once having our V[TCNE] film we then move on to determining weather or not dichloromethane solution will disrupt the magnetic order in V[TCNE] or if it will eliminate completely. First step is we will put the V[TCNE] samples in dichloromethane solvent solutions throughout different tie intervals. We add dichloromethane solvent in a glass bowl and add each film separately, one for 30 seconds, the next for five, ten, fifteen, and sixty minutes. Once completed adding dichloromethane we then move on to make Electron Paramagnetic Measurements to see which time affected V[TCNE] the most.

There are two ways of making measurements to find out what type of magnetic field the material has. One is Ferromagnetic Resonance FMR and the one we will be using is Electron Paramagnetic Resonance EPR. Although, EPR and FMR show the same signature data, FMR is a spectroscopic technique used to examine magnetization of ferromagnetic materials, whereas EPR examines paramagnetic materials (UnknownFM). EPR is a spectroscopy that provides different measurements than the Superconducting Quantum Interference Device SQUID which will later be discussed. **(image of EPR & FMR data)** The x-axis in EPR is the applied field measured. This is important because it shows what's changing in EPR. Field is related to a frequency that can be calculated using Larmor's Equation that is $\omega_{Larmor} = \frac{d\phi}{dt} = \frac{e}{2m_e}B$ this is calculating the resonant frequency (B) by the changes in frequency (**$d\Phi/dt$**) giving **ω** Larmor (Hyper Physics). The results may be familiar with paramagnetic materials.

One we ran our control and time samples of V[TCNE] through EPR. Figure 2 is a graph with amplitude on y-axis and exposure time on the x-axis. The graph helps us plot all out samples to help pick three best samples that have the most impact on the amount of magnetization. This is done so we can have three best samples including our control to run them through the SQUID. The SQUID measurements show local magnetic ordering of the applied field in the VTCNE films, which will be my main focus in this research.

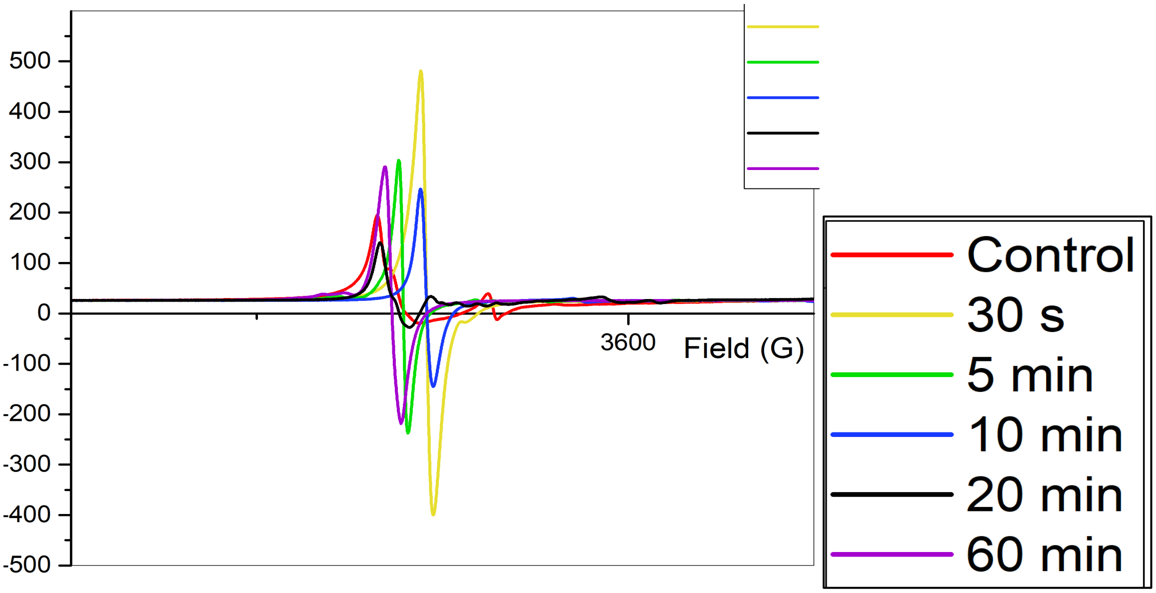

Figure 2. Graph of the time interval sample's of dichloromethane

Magnetic Property Measurements System MPMS is software designed to be a primary research tool in studies of magnetic matter it can execute magnetization measurements from different applied temperatures or fields. The thin films of V[TCNE] and dichloromethane solvents will be deposited one by one in quartz glass substrate tubes inside a plastic straw that are then moved down into superconducting coils that are connected to the SQUID. This will then provide a hysteresis loop and IR data that will identify the structure of the molecules. Part of the main goals is to test our dichloromethane solvent with V[TCNE] in the SQUID to help analyze the types of magnetic behavior it will have and weather our V[TCNE] is resistant or not.

For our SQUID data however showed different results than what our EPR was. In figure 3 you can see how our net magnetization was lost because it is showing a diamagnetism order meaning no net magnetization from our 30 sec sample and 20 min. This could have been caused by a variety of things that might have occurred throughout this experiment. Either transferring them from EPR to SQUID of the way the SQUID might have just measured our glass quartz tube instead of our sample also. The question continues to be unanswered.

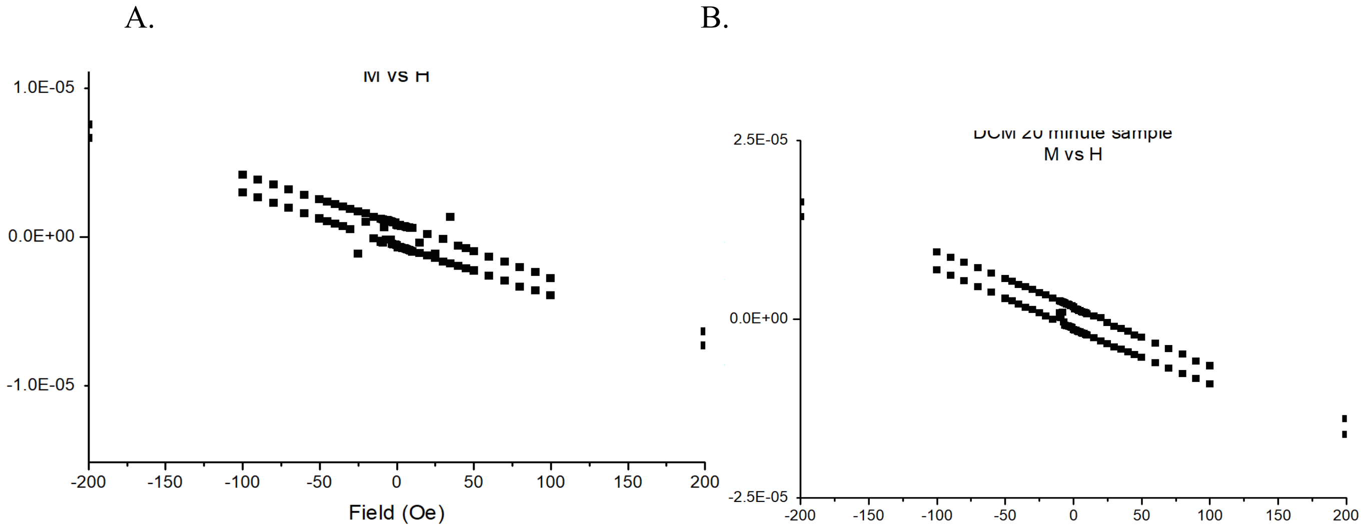

Figure 3. (A) 30 sec and (B) 20 min SWUID samples. Xaxis if applied field and y axis is our magnetization

Methods

- Grow V(TCNE)2 to prove that it can be grown in that 4way (involves a lot of smaller steps that have not been done yet)
    - Connecting both (V(CO)**6**) and TCNE into the Four way glass tube
    - Wrapping heat wire around (V(CO)**6**) T-boat to separate CO from vanadium.
    - Then adding Argon into it to help construct V[TCNE] together.
- Then measure the V[TCNE] in the Squid and FMR to record the control.
- Then add the dichloromethane solvent to V[TCNE]
- Lastly measure the V[TCNE] with the solvents in SQUID and FMR to see if there is any changes in V[TCNE] magnetic field.

Discussion

So given this data we are able to identify that our hypothesis was incorrect but our motivation was. Adding our V[TCNE] films into the dichloromethane solvent did not disrupt the magnetic order. However the question continues if there was something done wrong throughout the experiment that might have affected our samples when we switch them to measure them through the SQUID measurements. For our future work we will create double the V[TCNE] samples to help identify where this problem took place. So we will make before and after we add dichloromethane to help us analyze this problem better compared to our previous results.

References

F. Author & S. Author. Organic-based Magnetically Ordered Films. Retrieved from Ohio State University Physics Department.

Harberts et al. (2015). Chemical Vapor Deposition of an Organic Magnet, Vanadium Tetracyanoethylene. The Ohio State University Department of Physics and Chemistry.

Harberts, Megan. (2015). Materials engineering, characterization, and applications of the organic- based magnet, V[TCNE] (Doctoral dissertation). Retrieved from Ohio State University Physics Department.

Hyper Physics. (August 2000). Larmor Precession. Retrieved from: http://hyperphysics.phy-astr.gsu.edu/hbase/magnetic/larmor.html#c1)

Unknown: Ferromagnetic Resonance: Retrieved from: http://www.uam.es/personal_pdi/ciencias/farkhad/docencia/MASTER/12_13/guion_FMR_ingles.pdf

Thin-film Cu_2O Growth and Surface Structure on Cu (100): An STM Study

Andrew Lininger, Steven Tjung, Jay Gupta
Department of Physics, The Ohio State University

ABSTRACT

The growth and surface structure of thin-film Cu_2O on a crystalline Cu (100) surface has been studied through low temperature ultra-high vacuum scanning tunneling microscopy (UHV-STM). Two distinct regions are observed on the surface: adlayer terraces, exhibiting characteristic step edges of 4Å, and flat patches with a distinctive striped pattern. The adlayer is identified as oxidation of the Cu (100) surface through atomic resolution of the 'ladder' structure (missing-row reconstruction), with rectangular depressions on 3.7Å. The surface is observed under cold *in situ* dosing of CO_2. The flat striped patches are associated with the Cu_2O (111) surface, identified by two distinct patterns of protrusions: a (1x1) periodicity hexagonal lattice with spacing 3.1Å and an atomically resolved (√3x√3)R30° periodicity lattice with spacing of 5.2Å. The first structure is attributed to individual copper ions on the stoichiometric ideal (111) surface and the second to oxygen vacancies and the nearest-neighbor Cu atoms on the same surface. This demonstrates that similar structures occur on monolayer Cu_2O (111) as on the bulk Cu_2O (111) surface.

I. Background and Introduction

In order to understand and fully appreciate the properties and potential range of applications for Cu_2O, it is necessary to understand the surface structure and growth of the material at a fundamental level. This is desirable for several reasons, among them furthering the range of potential applications, such as catalysis of reactions[1], and applying knowledge to other similar and more complex structures. One major application is the production methanol from carbon dioxide[1], using copper oxide to catalyze the reaction. We expand upon previous work in this group oxidizing the Cu (100), and categorizing the structure. We attempt to grow a monolayer of Cu_2O on the Cu (100) surface and investigating the properties in relation to the oxidized surface.

Previous work in this group attempts to categorize the surface of an oxidized Cu (100) crystal. The missing row (2√2x√2) R45° reconstruction of the Cu (100) surface is observed, seen as a 'ladder' structure with a series of rectangular depressions and bright protrusions. The depressions occur in a regularly spaced array with two clearly separate domains oriented at 90° to one another. The results agree with corresponding DFT calculations.

We now move beyond characterization of the oxidized crystal surface to a monolayer of Cu_2O specifically grown upon the surface. One area of significance is the catalysis of methanol from carbon dioxide, which requires nanorods composed of both CuO and Cu_2O. To fully understand and realize this work, we must know the Cu_2O surface and its interaction with carbon dioxide deposition.

There have been previous accounts of the bulk Cu_2O (111) surface, and several distinct structures have been categorized. The configurations are hexagonal arrays: a (√3x√3)R30° surface reconstruction, and a (1x1) hexagonal reconstruction of the Cu_2O(111) surface.[2][3] The lattices are of periodicity 11Å and 5-7Å, respectively. This result is confirmed by means of scanning tunneling microscopy (STM) by Önsten, and low energy electron diffraction (LEED) by Schultz and Cox.

In the study by Schultz and Cox[3], the sample was first prepared by ion-bombarding and subsequent annealing of the $Cu_2O(111)$ surface. The (√3x√3)R30º reconstruction was obtained after annealing to 550ºC, while a hotter anneal of 950-1000ºC produced the (1x1) hexagonal periodicity. It is suggested the (√3x√3)R30º periodicity occurs as a result of oxygen vacancies on the surface, specifically a loss of 1/3 of the terminating oxygen anions; this conclusion supported by TDS and XPS data. The (1x1) periodicity is suggestive of a stoichiometric ideal surface, and TDS records oxygen vacancies at just 3% for the surface layer, supporting the stoichiometric ideal model of the surface.

Önsten *et. al.* report similar results.[2] They observe the (√3x√3)R30º periodicity after ion-bombardment and annealing to 600-730ºC, and the (1x1) periodicity after an anneal in high pressure O_2 ($2x10^{-6}$ mbar) at 650-700ºC, although the (1x1) lattice can be imaged at gaps in the (√3x√3)R30º lattice. They suggest the (√3x√3)R30º periodicity to be the product of an ordered loss of 1/3 of the surface oxygen, as confirmed by images of the relative size and non-uniformity of the lattice protrusions, and limited resolution of lattice substructure. Two explanations of the (1x1) periodicity are given: the stoichiometric ideal Cu(111) surface, or groupings of three Cu ions about an oxygen ion with vacancies in the under coordinated Cu ions. It has been reported that the second model represents a lower free energy than the stoichiometric ideal surface.[4]

There are several other possible structural patterns for the $Cu_2O(111)$ surface, observed with UHV STM.[5][6] Of interest is the '44' construction, which consists of a periodicity 22.0Å x 11.8Å unit cell commensurate with the 1x1 lattice. The lattice is interpreted as a deformation of the 1x1 hexagonal lattice caused by a mismatch with the substrate. The '44' structure is notable for its parallel stripes running the height of the patch, with separation on the order of 2.2nm.

Scanning tunneling microscopy is the main method used in investigation of the Cu_2O surface structure in this study. STM involves taking a sharp metal tip terminated by few atoms extremely close to a conducting sample. When the tip is sufficiently close to the sample there is a quantum mechanical probability for an electron to tunnel through the gap. A voltage potential is applied to the sample and the tip is grounded, to control the tunneling between the tip and sample. Assuming the tunneling probability we can calculate the rate at which tunneling occurs and thus define the tunneling current. We find the tunneling current decays exponentially with the tip-sample separation. Due to the strong dependence of tunneling current on distance, we can obtain a relative measurement of the tip-sample separation by measuring the tunneling current.[7]

To examine the 2-d surface of the material, the tip is mounted on a piezoelectric and swept in parallel scan lines across the surface. There are two scanning modes, constant current and constant height. In constant current mode the tunneling current is collected and fed through a feedback loop which adjusts the voltage controlling the vertical height of the tip, maintaining a constant tunneling current. The height control voltage can be collected and read as the topography of the surface. Constant height mode has a limited range of applicability given the necessity for a relatively flat surface. Here the height is fixed and the tunneling current is collected while scanning; the current is read in much the same way as before. Thus assuming a relatively constant conductivity in the material we can confidently understand the surface structure of our material. STM is ideal for this study, as we require topographical fine resolution of a conducting and few-layer semi-conducting material.

Figure 1: Scanning tunneling microscopy. A sharp metal tip is brought close to the surface, inducing a tunneling current. We can scan to image a topography of the surface, and manipulate the surface with an electric field from the tip.

One important consideration is that the STM probes the electronic structure of both the tip and sample, which is not necessarily the same as the topographical structure. However we can make some simplifying assumptions to justify the estimation. First we assume the charge to be spherically symmetric around the nucleus, although there is some debate over the charge structure of Cu_2O.[2] We also assume the effect of surface states to be negligible, as the predicted states are well away from the Fermi level.[2]

II. Methods

All experiments were carried out in ultra-high vacuum (10^{-10} mbar) in both chambers, and without breaking vacuum between preparation and STM imaging. Imaging was conducted in a Createc UHV-STM, cooled to 5K. All STM imaging was conducted in constant current (topography) mode. The temperature of the sample was measured with a thermocouple mounted slightly above the sample, and thus an inaccuracy in the temperature reading was introduced. Annealing of the sample was also limited by the capacity of the serpentine heater, reaching a maximum of 250ºC. Copper deposition was achieved through *e*-beam evaporation and O_2 deposition through pressurization of the chamber.

The sample was first cleaned through three cycles of Argon sputtering (10^{-5} mbar Ar) and annealing up to 240°C, in 10 minute cycles. The Cu(100) sample was then subjected to 2 minutes of exposure from a Cu evaporator in pressurized oxygen ($2\text{x}10^{-6}$ mbar O_2), while being heated to 240°C. The growth was confirmed by auger spectroscopy in the preparation chamber directly following the growth, to determine a suitable method for the deposition. For imaging runs, immediately following the growth the sample was annealed at 240°C while pumping out the O_2 for a clean anneal. The pressure decrease was sufficiently rapid. After LN_2 cooling (~30 minutes), the sample was transferred directly into the STM chamber to minimize contamination on the surface. To study molecular deposition on the surface, the sample was exposed *in situ* to high pressure ($2\text{x}10^{-6}$ mbar) CO_2 for 5 minutes without heating the sample.

III. Results and Discussion

1. Cu_2O growth conditions

In determining the optimal growth method the sample was subjected to the growth conditions for varying amounts of time and under varying annealing conditions. Auger spectroscopy was taken on the sample after each growth run in order to determine the relative amount of each Cu and O on the surface and thus estimate the coverage. Continued Cu_2O growth on the surface produces changes in the relative intensity of the Cu and O auger peaks, as we are receiving more signal from the Cu_2O rather than Cu or the oxidized Cu surface. Therefore during this growth a change in the relative intensity of Cu and O peaks can be interpreted as a change in the Cu_2O surface coverage. Further growth without any change indicate coverage in previously covered areas. However complete surface coverage would result in multilayer deposition in some areas, so by necessity a monolayer will be partial coverage. We also desire partial coverage in order to compare the grown Cu_2O regions with the underlying oxidized copper regions. Thus we attempt partial monolayer coverage of the surface by growing just until a change no significant in peak intensity is observed.

The auger results are seen in figure 2. It was found that for the clean Cu (100) sample, exposures longer than two minutes did not result in a significant change to the relative intensity of Cu and O peaks, indicating that the surface to be adequately covered with monolayer oxide. Subsequent growth serves only to build thicker films, not desired for this project.

The anneal following the growth was designed to allow material on the surface to settle and continue self-assembly. It was found that increasing the length of anneal from 1 to 5 minutes at 240°C did not substantially clean the surface. We were unable to anneal any hotter due to limitations of the heater; a hotter anneal might do better to clean the surface.

Figure 2: Auger spectra of copper oxide growth. Growth was preformed in 1 minute intervals of deposition. The ratio of Cu/O peak intensity changes between the first two, but stays constant between the second and third growth.

Figure 3: a) Adlayer lattice structure, with CO_2 molecules adsorbed on the surface (right middle). b) Stacked adlayer terraces (5 levels) with jagged step edges. c) Clear missing-row reconstruction of Cu (100) surface, with a few defects. d) Atomic interpretation of the surface ladder structure, left overlay of the atomic structure on the lattice.
[Imaging: 0.6V/2nA]

2. Adlayer

An example of the observed adlayer structure is shown in figure 3a. A clear atomic 'ladder' structure characteristic of the missing row reconstruction is observed, indicating a (2√2x√2)R45° reconstruction of the Cu (100) surface. The spacing between depressions are envisioned as rungs on the ladder, and occur with periodicity 3.7Å. Two domains are observed, with a 90° orientation to each other, and identical spacing. The structure is also clearly defined, and appears to remain highly coordinated in its long range order. Given that these results are concomitant with those previously observed on the oxidized Cu (100) surface, we again associate the adlayer structure with the uncovered oxidized surface of the crystal. This result is understood in terms of the growth procedure: the Cu (100) surface is exposed to high pressure O_2 for a short time before the Cu deposition, leading us to expect a similar oxidized structure on the (100) crystal surface before any growth.

The atomic pattern is observed on large flat adlayer terraces, as seen in figure 3b. These terraces are terminated in step edges, typically with an apparent 4Å drop, although some different heights are observed, but always in multiples of 2Å. The typical 4Å step height corresponds to a double copper step. The edges of the steps appear as a stretch of jagged edges, often as right angles, as seen in figure 3b. The right angles in the step edges are suggestive of an underlying square lattice, as observed at the atomic scale.

Obtaining atomic resolution of the adlayer structure, the chamber is then flooded with CO_2 to observe the deposition and orientation of molecules on the surface. The sample was kept at 5K throughout the deposition and subsequent imaging. The surface after deposition can be seen in figure 3a, where the small white spots on the right side correspond to adsorbed CO_2 molecules. The adsorbed molecules prefer to align in and parallel to the missing rows of the reconstruction, with an apparent height ~0.8Å above subsequent depressions. The CO_2 molecule is linear, and appears to sit with the central C atom in the hole between the missing rows. The adsorbed CO_2 molecules on the adlayer surface can be manipulated through interaction with the tip. Molecules can be moved about the surface with scanning under normal conditions, about 0.6 V and 2nA, indicating the molecules are relatively weakly bound to the surface.

3. Cu_2O (111) stripes and structure

Between the adlayer terraces are large regions with parallel stripes running the length; subsequent stripes are separated by roughly 8nm. See figure 4. These regions maintain a relatively constant height, to the order of an angstrom. They are wide, generally around 100nm, and several times as long. The stripes always occur at 20° to the adlayer lattice on the jagged step edges, and are seen to cut around corners at 120°. See figure 4b.

The relatively constant order in the height and constant angle and spacing between stripes speaks to some underlying structure to the patches. However these patches appear disordered at close range during this phase, and spectroscopy is unreliable on the surface because of instability. The observed disorder is categorized as a large number of random vacancies in the lattice, resulting in a large number of under-coordinated Cu and O atoms in the lattice. This structure is a result of the low temperature at which the sample was annealed after growth. Lower temperatures do not allow the under-coordinated atoms enough energy to arrange themselves into a complete lattice, resulting in vacancies and an under-developed structure. Annealing was limited at ~240°C by the sample heater, which is much lower than previous attempts with the bulk crystal surface. It is hypothesized that a higher temperature anneal will allow the assembly of atoms into the lattice. The stripes are thought to be the result of buckling of the patch, and not a direct feature of the lattice structure, albeit along the underlying lattice.

Two distinct atomic resolved lattices are observed for Cu_2O in the striped region, by using a sweeping technique. See figure 5. Quick, high bias (~4V) scans are employed to move atoms on the surface moving atoms away and possibly into or out of the lattice. The first observed lattice is a a similar (1x1) periodicity hexagonal lattice, with protrusions on 3.1Å. This lattice is observed most commonly throughout the areas imaged, and at an annealing temperature much lower than that necessary to obtain the structure on the bulk surface. The known structure of Cu_2O (111) exhibits a nearest neighbor spacing of 3.02Å for first-layer Cu_A atoms, and 6.04Å for O atoms, with the atoms arranged in a (1x1) hexagonal pattern in the plane. See figure 5a. The (111) plane has only one type of ion (Cu^+ or O^{2-}) in each plane.

We observe a (1x1) periodicity lattice with a spacing of 3.1Å. There are two options to explain this result, the stoichiometric ideal (111) surface with protrusions corresponding to regularly spaced Cu_A ions, or more complicated protrusions corresponding to groups of three second-layer Cu_B ions. The stoichiometric ideal surface is energetically favorable, and we image the protrusions as homogeneous points without resolved substructure. With these results there is not enough evidence to justify the second interpretation, and we conclude the observed lattice to be imaging of Cu_A ions on the stoichiometric ideal (111) surface. This result could potentially be revised by atomic resolution of the protrusions, and this is an avenue for future work in this area.

Figure 4: a) Striped patch grown on top of flat adlayer terrace, left side. b) Stripes can go around a corner at a constant angle, and new stripes are created in the bend. c) Striped region against higher step edges, stripes at a constant angle with respect to the adlayer. [Imaging: 0.6V, 2nA]

The next atomic lattice structure observed is a $(\sqrt{3}x\sqrt{3})R30^{o}$ reconstructed hexagonal lattice of donut-like protrusions, separated by 5.2Å. See figure 5b. This structure is obtained in the same way as the previous. An important clue to the structure of the $(\sqrt{3}x\sqrt{3})R30^{o}$ periodicity hexagonal structure is seen in figure 5c. The atomically resolved protrusions are inhomogeneous, meaning they must consist of several ions, although the exact structure is beyond our current resolution. Also this structure is observed in the same patches as the previous (1x1) lattice, and thus we are relatively certain we are looking at Cu_2O (111) and this lattice must correspond some perturbation of the (111) structure. Another check is the orientation of the ideal (111) lattice with the adlayer, which is found to be 20°. This result agrees with our measurement of the stripe orientation, and confirms we are really looking at Cu_2O (111).

Figure 5: a) P2 protrusions: resolved (1x1) hexagonal lattice, with atomic points marked. b) P1 protrusions: resolved hexagonal lattice of donut-like protrusions. c) Model of Cu_2O (111), with P2 lattice marked in green. d) Model of Cu_2O (111), with oxygen vacancies represented by blue circles and protrusions outlined in yellow. [Imaging: 0.6V, 2nA]

Figure 6: a) P2 lattice on the Cu_2O (111), with adlayer lattice in the bottom left corner; clear overlay. b) Image of the same area as (a), lattice overlays drawn over both structures. Lines on the overlay represent direction of lattice. Angle between lattices confirms earlier result. [Imaging: 0.6V, 2nA]

The best explanation for these protrusions is the oxygen vacancy model in which groups of six Cu_A and Cu_B ions on Cu_2O (111) are formed about an oxygen vacancy in the $(\sqrt{3}x\sqrt{3})R30^o$ position, with 1/3 or 2/3 of the surface oxygen removed. See figure 5d. Protrusions in the images correspond to these 6 Cu ions around the O vacancy, and the spacing of vacancies gives rise to the lattice pattern. Such a conclusion is understandable given the disordered state of the patch from which the structure arises, although this structure was found to occur under the same conditions as the first. In accordance with Önsten, and Schultz and Cox working with the bulk surface, the structure is attributed to this model.

IV. Conclusions

We investigate the growth and structure of monolayer Cu_2O on Cu(100) using STM imaging. The optimum growth conditions are determined for the sample. Imaging yields two different regions on the oxide surface; adlayer terraces with a distinct atomic ladder structure, and patches of Cu_2O with a large-scale patter of parallel stripes. The terraces correspond to those seen before for the oxidized reconstruction of the Cu(100) surface. Two atomic patterns are observed in the striped region, attributed to the Cu_2O (111) plane: a $(\sqrt{3}x\sqrt{3})R30^o$ periodicity lattice with 5.2Å spacing, which is determined to be the result of groups of six Cu ions forming about an oxygen vacancy at the $(\sqrt{3}x\sqrt{3})R30^o$ position, and a (1x1) periodicity lattice with a 3.1Å spaced hexagonal pattern, which is determined to be the stoichiometric ideal Cu_2O(111) surface. The first lattice represents an ordered loss of 1/3 of the surface oxygen, while the second represents individual Cu ions on the (111) surface. Imaging of the protrusion substructure in the first case resolves inhomogeneity, justifying the characterization. No such resolution could be obtained for the second lattice protrusions, and this is a potential check on the interpretation. Other possible improvements include annealing the sample to higher temperatures, in an attempt to clean the Cu_2O surface and reach those temperatures obtained by Önsten, and Schultz and Cox, obtaining better resolution of the oxygen vacancy protrusions to confirm the structure, and categorizing the stripes observed on the Cu_2O(111) surface. These results are concomitant with previous observations of the bulk Cu_2O (111) surface, and this observation of monolayer Cu_2O confirms that many of the same structures are found in both cases.

V. Acknowledgments

We would like to thank the Center for Emergent Material at The Ohio State University, and the NSF. The REU program is part of an NSF Materials Research Science and Eng-ineering Center (MRSEC) supported under NSF Award Number DMR-1420451.

VI. Footnotes, Endnotes and References

[1] G. Ghadimkhani, *et. al.*, *Chem. Commun.* **49**, 1297 (2013).
[2] A. Önsten, M. Gothelid, U. O. Karlsson, *Surface Science* **603**, 257 (2009).
[3] K. H. Schultz, D. F. Cox, *Phys. Rev. B* **43**, 1610 (1991).
[4] A. Soon, M. Todorova, B. Delley, C. Stampfl, *Surface Science* **601**, 5809 (2007).
[5] F. Jensen, F. Besenbacher, E. Laegsgaard, I. Stenegaard, *Surface Science Let.* **259**, L774 (1991).
[6] A. Baber, *et. al.*, *J. Am. Chem. Soc.* **135**, 16781 (2013).
[7] J. Stroscio, W. Kaiser, (1993). *Methods of Experimental Physics. Volume 27. Scanning Tunneling Microscopy*. Boston: Academic Press.

Notes on Quantum Spin Liquids

July 28, 2017

Summary: One of the topics examined this summer was quantum spin liquids. In low temperature systems, there are two competing effects that influence magnetic order: classical ordering and quantum fluctuations. In antiferromagnetic materials, this "battle" between quantum and classical effects is usually won by antiferromagnetic interactions, resulting in a Néel ordered state at low temperatures. However, in certain materials, the quantum paramagnetic phase persists all the way to zero temperature, forming an exotic state of matter called a quantum spin liquid (QSL).

Background

A universal phenomenon found across all condensed matter systems is the tendency for materials to freeze out their degrees of freedom at low temperatures. Probably the most well-known instance of this is liquids freezing to form solids below their melting points. However, other properties of substances are also able to order at low temperatures. An important example occurs with magnetic ordering, or the arrangement of the individual magnetic moments (spins) in a material. Just as most materials will freeze into a crystalline phase when cooled, so too will their magnetic moments, producing long-range order.

For conventional condensed matter systems, there are two primary forms of magnetic ordering: ferromagnetic and antiferromagnetic. In ferromagnetic materials, the magnetic moments will spontaneously align with each other below the Curie temperature, resulting in a net magnetization of the material. This is in contrast with antiferromagnetic interactions, where neighboring spins point antiparallel below the corresponding Néel temperature. A Néel ordered state produces no net magnetization.

Representation of Ferromagnetic and Antiferromagnetic States

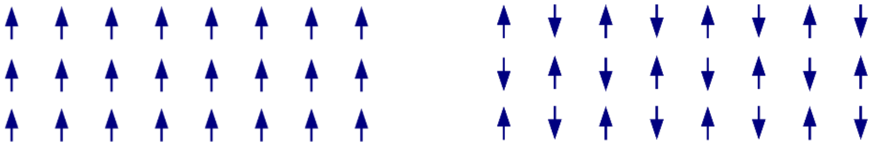

In the cases of ferromagnetic and antiferromagnetic ordering, the magnetic moments break a continuous symmetry and settle into a static configuration at temperatures below their critical temperature. A question of significant theoretical and practical interest is whether there exist materials that do not fall into either of these categories, that is, are there materials that do not magnetically order even at arbitrarily low temperatures? For a long time, the answer was assumed to be no. However, experiments in the past ten years have discovered what appear to be "quantum spin liquid" states, leading to a recent surge in theoretical activity attempting to understand and characterize these materials.

Quantum Spin Liquids

A quantum spin liquid (QSL) is defined as a state of matter where the spins resist ordering at temperatures down to 0 K. This effect is possible due to the presence of strong destabilizing quantum fluctuations (zero-point motion courtesy of the Heisenberg uncertainty principle). A simple model that is often used in the study of quantum magnetism is the Heisenberg Hamiltonian:

$$H = J \sum_{<i,j>} \vec{S}_i \cdot \vec{S}_j$$

where J is the coupling constant given by the exchange integral, S_i and S_j are spin operators, and $<i,j>$ denotes a sum over nearest neighbors on a lattice.

In the Heisenberg model, there are three parameters that can be varied: the coupling constant, the spin size, and the lattice geometry. At temperatures on the order of the coupling energy, these parameters dramatically influence the system's magnetic properties. Quantum spin liquids in particular are favored by an antiferromagnetic coupling constant, a small spin magnitude, and a combination of low dimensionality and high frustration in the lattice arrangement. Each of these effects is described in greater detail in the following sections.

Coupling Constant

The sign of the coupling constant between neighboring spins is central to spin liquid realization. In a ferromagnetic material ($J < 0$), the ground state is trivially one where all spins point in the same direction. This property of ferromagnetic interactions is independent of lattice shape, and no amount of quantum fluctuations are able to destabilize the ground state. Hence, ferromagnets cannot become quantum spin liquids. Antiferromagnetic materials ($J > 0$) are more interesting. Their classical ground state is a Néel ordered state, but quantum mechanically, they can produce a ground state consisting of spin singlet pairings which are crucial to spin liquid formation. Hence, a positive coupling constant is a necessary condition for a material to produce a quantum spin liquid state.

Spin Size

Another important factor for the formation of quantum spin liquids is a low spin. Since the commutator of two spin operators is proportional to 1/S when normalized by size, spin systems act classically in the large S limit. QSLs are the result of quantum mechanical fluctuations, so spin systems in the low S, quantum regime (spin-1/2 in particular) are most likely to result in a spin liquid state.

Dimensionality

Although all physically realizable systems are three-dimensional, it is often the case that couplings are mostly axial or planar leading to materials that can be approximated as one or two-dimensional. In these low dimension systems, lattice sites have fewer neighboring magnetic moments (lower coordination numbers), which tends to favor quantum disordered states over Néel ordering.

Lattice Frustration

Antiferromagnetic coupling paired with low spin and dimensionality alone is generally not sufficient to prevent magnetic ordering at T = 0; lattice geometry has to also conspire to produce a QSL state. Indeed, even in the extremely favored of 1D Heisenberg spin-1/2 chain, the spin-spin correlation function decreases slowly as ~1/r. In contrast, the spin-spin correlation for thermal magnets is an exponential decay.

A final key ingredient, lattice frustration, is needed to produce a quantum spin liquids. Lattice frustration is a geometric property of lattices that occurs when the underlying lattice structure prevents antiferromagnetic spin interactions from being satisfied. Without frustration, 2D and 3D systems will Néel order into a bipartite lattice, eliminating the possibility for a QSL. Lattice frustration can most easily be seen in the case of an antiferromagnetic triangular lattice, shown in the figure below. It is clear that once the first two lattice sites have satisfied their antiferromagnetic couplings, there is no positioning of the third spin that results in all three interactions being simultaneously satisfied. The third lattice site is "frustrated" and has no unique ground state.

Frustration on a triangular lattice

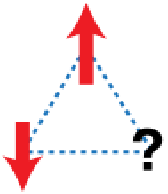

An important property of frustrated lattices is that they lead to a very large degeneracy of ground state. Even in system with only three lattice sites, there already exists a six-fold degeneracy of the ground state. These configurations for a three-site system are shown below.

Degeneracy due to AF interactions on a frustrated lattice

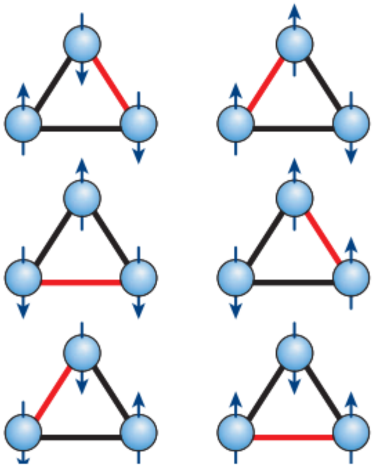

In addition to the triangular lattice, the two-dimensional kagome lattice is nearest-neighbor frustrated. In three dimensions, the pyrochlore lattice, consisting of corner sharing tetrahedral, exhibits a high degree of frustration. Frustration may also be introduced to other lattice structure in the form of next-nearest neighbor couplings or via anisotropic interactions. Pictorials of the kagome and pyrochlore lattice structures can be found below.

Kagome

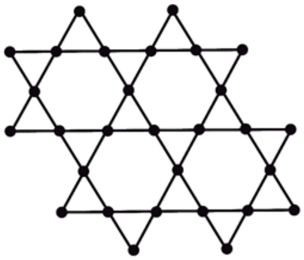

Pyrochlore

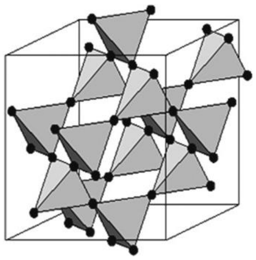

Frustration upsets the tendency for magnetic systems to Néel order into a bipartite lattice. However, theoretical calculations indicate that the low temperature ground state of a triangular lattice is actually a *three-part* sub lattice. The pyrochlore lattice has been difficult to study theoretically because the 3D nature of the lattice makes numerical simulations impractical for anything more than a few sites. As such, the most intense research attention has been directed towards the kagome lattice; its high degree of frustration and two dimensionality make the spin-½ kagome lattice the most promising lattice geometry for a quantum spin liquid. Evidence in support of a QSL being the ground state for the kagome lattice includes calculations demonstrating nonzero entanglement entropy as well as density matrix renormalization group studies showing a spin gap.

A useful quantitative measure of lattice frustration is given by the Ramirez frustration parameter: $f = -\theta_{CW}/T_N$, where Θ_{CW} is the Curie-Weiss temperature (negative for antiferromagnets) and T_N is the Néel ordering temperature. A value of f >> 1 indicates a high degree of frustration and can identify promising candidates for spin liquid systems.

Resonating Value Bond Theory

The ground state of two antiferromagnetically interacting $S = \frac{1}{2}$ spins is a valence bond singlet pair with total spin zero. A many body state can be formed from the direct product of these singlet pairs. This dimer covering of the lattice is called a valence bond crystal (VBC), and although a VBC is non-magnetic, its singlet pairs still break the lattice symmetry. This retention of magnetic order prevents a VBC from becoming a quantum spin liquid. However, if there is enough frustration present in the lattice, it is theorized that the system will be able to quantum mechanically tunnel among the many degenerate VBC ground states, with each spin constantly breaking and forming singlet pairs. Such a superposition state is called resonating valence bond (RVB) state, and it was first suggested by Anderson as an alternative to Néel ordering at low temperature. The result is a highly entangled and nonlocal many-body wavefunction that cannot be written as a product of individual states. A RVB state is a true quantum spin liquid, because the superposition of VBC states restores symmetry to the system.

Experiment

Of all the thousands of antiferromagnetic materials that have been studied, almost all have exhibited magnetic ordering at low temperatures. To date, there have been no clear experimental confirmations of the existence of QSLs. However, the past decade has seen some very important experimental work on QSLs, and multiple materials have been identified as quantum spin liquid candidates. One particularly strong candidate is herbertsmithite ($ZnCu_3(OH)_6Cl_2$), a mineral that forms a 2D $S = ½$ kagome lattice. In other words, herbertsmithite manifests a nearly perfect realization of theoretical QSL predictions. Measurements down to temperatures as low as 50 mK have found herbertsmithite to exhibit all the characteristic features of a QSL.

There are a number of experimental probes that can be done to look for the presence of a quantum spin liquid. One technique is neutron scattering, which offers a direct probe into the spin-spin correlations in a sample. In herbertsmithite, neutron scattering has shown that its excited states at low temperatures are exotic fractional spin excitations called spinons, a hallmark of the QSL state of matter. Another experimental probe is specific heat measurements. A quantum spin liquid can support a large number of gapless excitations due to its massive degeneracy, leading to anomalously high specific heats. Specific heat measurements can also be used to determine entropy, which can then be compared against theoretical models. The downside to the specific heat technique is that it is not always clear what type of excitations one is measuring. Magnetic susceptibility measurements offer an additional indicator for QSLs through its impact on the Curie-Weiss temperature, and thereby the frustration parameter. NMR, μSR, and X-ray scattering can also offers experimental clues for a quantum spin liquid.

Applications

Quantum spin liquids possess a diverse and exciting set of properties that are very interesting theoretically, but they may also have applications in other areas of research. Among these potential applications is superconductivity, where the resonating valence bond state has been proposed as a mechanism for high temperature superconductivity. Additionally, the ability of quantum spin liquids to sustain topologically-protected states that remain entangled at long distances suggests a potential application in quantum computers, where there is a need for scalable and fault-tolerant error correction.